https://doi.org/10.5194/acp-2020-1298
Preprint. Discussion started: 25 February 2021

Atmospheric Chemistry and Physics Discussions

OMI-observed HCHO in Shanghai, China during 2010-2019 and ozone sensitivity inferred by improved HCHO/NO_2 ratio

Danran Li [1], Shanshan Wang [1,2], Ruibin Xue [1], Jian Zhu [1], Sanbao Zhang[1], Zhibin Sun[1], and Bin Zhou [1,2,3]

[1]Shanghai Key Laboratory of Atmospheric Particle Pollution and Prevention (LAP[3]), Department of Environmental Science and Engineering, Fudan University, Shanghai, China
[2]Institute of Eco-Chongming (IEC), No. 20 Cuiniao Road, Shanghai 202162, China
[3]Institute of Atmospheric Sciences, Fudan University, Shanghai, 200433, China

Correspondence to: Shanshan Wang (shanshanwang@fudan.edu.cn)

Abstract. In recent years, satellite remote sensing has been increasingly used in the long-term observation of ozone (O_3) precursors and its formation regime. In this work, formaldehyde (HCHO) data from Ozone Monitoring Instrument (OMI) were used to analyse the temporal and spatial distribution of HCHO vertical column densities (VCDs) in Shanghai from 2010 to 2019. HCHO VCDs exhibited the highest value in summer and the lowest in winter, the high-VCD concentrated in western Shanghai. Temperature largely influence HCHO by affecting the biogenic emissions and photochemical reactions, and industry was the major anthropogenic source. The satellite observed formaldehyde to nitrogen dioxide ratio (FNR_{SAT}) reflects that the O_3 formation regime had significant seasonal characteristics and gradually manifested as transitional ozone formation regime dominated in Shanghai. The uneven distribution in space was mainly reflected as the higher FNR_{SAT} and surface O_3 concentration in rural area. To compensate the shortcoming of FNR_{SAT} that it can only characterize O_3 formation around satellite overpass time, correction of FNR_{SAT} was implemented with hourly surface FNR and O_3 data. After correction, O_3 formation regime showed the trend moving towards VOC-limited in both time and space, and regime indicated by FNR_{SAT} can better reflect O_3 formation for a day. This study can help us better understand HCHO characteristics and O_3 formation regime in Shanghai, and also provide a method to improve FNR_{SAT} for characterizing O_3 formation in a day, which will be significant for developing O_3 prevention and control strategies.

1 Introduction

Formaldehyde (HCHO) is an important trace gas in atmosphere. It has the irritating effect on human eyes, skin, and respiratory mucosa, and can also cause cancer in high concentration (Zhu et al., 2017a; Liu et al., 2018). Atmospheric HCHO is an intermediate product of almost all volatile organic compounds (VOCs) oxidation, it can be therefore indicative of the overall VOCs level (Chan et al., 2019). HCHO can also be emitted through anthropogenic sources, biogenic sources, and biomass combustion. Anthropogenic sources like transportation, power, industry, and residential etc. increase the amount of HCHO by emitting VOCs into the atmosphere (Wang et al., 2017). In addition, biogenic volatile organic

https://doi.org/10.5194/acp-2020-1298
Preprint. Discussion started: 25 February 2021

Atmospheric Chemistry and Physics Discussions

compounds (BVOCs) are also important sources of HCHO. Isoprene emitted by plant can be oxidized to generate HCHO, which causes the concentration of HCHO in some lush vegetation areas to be largely affected by emission of BVOCs (Millet et al., 2008). The removal of HCHO is mainly through photolysis, reaction with OH radicals and the deposition (Ling et al., 2016; Xing et al., 2020).

Satellite remote sensing can achieve large-scale observation of atmospheric pollutant gases including HCHO, which has been widely used in recent years. Sensors currently available for HCHO observation include the Global Ozone Monitoring Experiment (GOME) on ERS-2 (Burrows et al., 1999; Martin et al., 2004b), Scanning Imaging Absorption Spectrometer for Atmospheric Chartography (SCIAMACHY) on ENVISAT (Bovensmann et al., 1999; Stavrakou et al., 2009), Ozone Monitoring Instrument (OMI) on Aura (Levelt et al., 2006; Zhu et al., 2017b), GOME-2 on METOP as the successor of GOME (Callies et al., 2000; De Smedt et al., 2012), Ozone Mapping and Profiler Suite (OMPS) on Suomi-NPP (Su et al., 2019), and Tropospheric Monitoring Instrument (TROPOMI) on Sentinel-5P (Veefkind et al., 2012; Vigouroux et al., 2020). OMI can provide daily data of HCHO with higher spatial resolution (13 km×24 km). As a new generation of sensors, TROPOMI was launched in 2017, it has better spatial resolution (7 km×7 km) but lacks long-term observation so far. It would be an advantageous tool of satellite remote sensing to achieve more detailed analysis in the future (Veefkind et al., 2012).

Previous studies reported satellite observed long-term and large-scale distribution and variation of HCHO in China and all over the world (Millet et al., 2008; Zhu et al., 2017a; Liu et al., 2020). Twelve years observation of multi-satellite (OMI, GOME-2, SCIAMACHY) showed that the trend of HCHO vertical column densities (VCDs) over eastern China is consistent with that of anthropogenic VOCs (Shen et al., 2019). Based on 10 years observation of OMI HCHO, Liu et.al (2018) indicated that high HCHO VCDs in tropical forests region are greatly affected by biomass burning and meteorological factors including temperature and precipitation. In addition, the ground-based remote sensing can also be available for HCHO observation, such as the multi axis differential optical absorption spectroscopy (MAX-DOAS) measurement. The vertical distribution of HCHO derived from MAX-DOAS measurement was characterized by the higher HCHO concentrated near the surface (Lee et al., 2015; Chan et al., 2019). By employing the box model, Li et al. (2014) found that isoprene oxidation initiated by OH radicals have a great contribution to the HCHO formation in semi-rural region of the Pearl River Delta (PRD) in China.

HCHO participates in the complex photochemical reaction of NO_x (NO_x= NO + NO_2) and directly affects the production of O_3 in troposphere. Due to the short lifetime of HCHO and NO_2, their spatial distributions were greatly affected by local emission of VOCs and NO_x, which received widespread attention as precursors of tropospheric O_3 (Zaveri et al., 2003; Chan et al., 2019). Consequently, HCHO and NO_2 can be assumed as indicators of VOCs and NO_x, and the ratio of formaldehyde to nitrogen dioxide (HCHO/NO_2, FNR) can be an indicator to analyse the O_3 formation regime (Sillman, 1995; Martin et al., 2004a; Schroeder et al., 2017). For instance, by using FNR from long-term OMI HCHO and NO_2 data, O_3 sensitivity of the United States was evaluated. O_3 formation regime can be designated as VOC-limited for FNR < 1, NO_x-limited for FNR > 2, and transition for 1 < FNR < 2, which serves as the transitional regime between VOC-limited and NO_x-limited regimes,

https://doi.org/10.5194/acp-2020-1298
Preprint. Discussion started: 25 February 2021

Atmospheric Chemistry and Physics Discussions

indicating the production of O_3 can be changed by both VOC and NO_x (Duncan et al., 2010). In view of China, OMI products over three representative regions (North China Plain (NCP), the Yangtze River Delta (YRD) and the PRD) were investigated, revealing that the O_3 formation regime varied in both time and space, and the contribution of emission sectors to precursors changed with the type of regimes (Jin and Holloway, 2015). During special events such as Asia-Pacific Economic Cooperation in 2014 and Grand Military Parade in 2015, FNR in Beijing had become higher compared with previous periods, and the O_3 formation regime shifted toward NO_x-limited regime with control strategies (Liu et al., 2016).

In this study, OMI satellite data were used to investigate the temporal and spatial distribution characteristics of atmospheric HCHO in Shanghai from 2010 to 2019, combined with meteorological data and emission inventories to analyse the influencing factors. FNR calculated by satellite HCHO and NO_2 were applied to capture variation of the O_3 formation regime in Shanghai over the past decade. Considering that satellite data only reflect the column density of trace gas around overpass time, hourly surface FNR and O_3 concentration increment were proposed to correct the satellite FNR, so that it can better indicate O_3 formation in a day.

2 Data and Methods

2.1. Satellite data

OMI on Aura orbits the earth in about 98 minutes, which can achieve full coverage of the earth in one day. It overpasses at 13:45 local time (LT) each day. The scanning width is 2600 km, and is divided into 60 pixels. The sensor contains 3 channels, including UV-1, UV-2, and VIS, with a wavelength coverage of 264~504 nm. This band allows to observe a variety of trace gases, e.g., HCHO, NO_2, and SO_2 (Zhang et al., 2019). The retrieval algorithm of this product is based on nonlinear least-squares fitting which get slant column density (SCD) as the result. Then SCD can be converted to VCD through Air Mass Factors (AMF). The Level-2 OMI HCHO product OMHCHO Version-3 is used in this study (https://disc.gsfc.nasa.gov). Since atmospheric HCHO is mainly distributed in the troposphere, the total VCD can be regarded as the tropospheric VCD of HCHO (Duncan et al., 2010). The Level-2 OMI NO_2 product OMNO2.003 Version-4 is adopted as tropospheric NO_2 VCD in this study (https://disc.gsfc.nasa.gov).

2.2. Methodology

In order to ensure data quality, HCHO data with cloud fraction ≤ 30%, solar zenith angle ≤ 70°, and Main Data Quality Flag = 0 were selected in this study. In addition, the quality of pixel data with large size is poor, so 5 marginal pixels on each side were abandoned, and only pixel data within 6~55 were selected (Zhu et al., 2017a; Xue et al., 2020). Because OMI has experienced row anomaly since 2007, Xtrack flag = 0 was required to eliminate the influence of poor quality data affected by row anomaly (http://projects.knmi.nl/omi/research/product/rowanomaly-background). As HCHO satellite data have large error, fitting root mean square (RMS) ≤ 0.003 was limited to remove most outliers (Souri et al., 2017). The selection of NO_2 satellite data was basically the same as that of HCHO, but without fitting RMS parameter filtering, and cloud radiance

https://doi.org/10.5194/acp-2020-1298
Preprint. Discussion started: 25 February 2021

Atmospheric Chemistry and Physics Discussions

fraction ≤30% was required (Krotkov et al., 2016). After filtering, the pixel data were gridded to the spatial resolution of 0.01°× 0.01° for further discussion (Xue et al., 2020).

2.3. Auxiliary data

The meteorological data, including monthly temperature, sunshine hours, precipitation, and relative humidity are acquired from the National Bureau of Statistics of China (http://www.stats.gov.cn/). Hourly temperature data at Shanghai Hongqiao INTL Site (31.20°N, 121.34°E) come from the National Climatic Data Center (NCDC, https://www.ncdc.noaa.gov/). The anthropogenic sources of HCHO in Shanghai are calculated based on the China Multi-resolution Emission Inventory (MEIC, http://www.meicmodel.org/). Surface HCHO and NO_2 concentrations were measured by long-path differential optical absorption spectroscopy (LP-DOAS) at the Jiangwan campus of Fudan University in Shanghai (31.34°N, 121.52°E). The O_3 data of Qingpu Dianshan Lake Site (31.09°N, 120.98°E) and Hongkou Site (31.30°N, 121.47°E) in Shanghai are obtained from the Shanghai Environmental Monitoring Center (http://www.semc.com.cn/aqi/Home/Index).

3. Results and Discussion

3.1. The temporal and spatial variation of HCHO

HCHO VCDs for annual, monthly and seasonal variations in Shanghai from 2010 to 2019 are shown in Fig. 1. HCHO VCDs decreased from the highest value of 12.29×10^{15} molec·cm^{-2} in 2010 to the lowest value of 9.97×10^{15} molec·cm^{-2} in 2012, then rebounded from 2012 to 2014, and fluctuated slightly in the following years (Fig. 1a). The column value and variation are similar to previous study in the YRD, China (Zhang et al., 2019). Before 2018, the high-VCD concentrated in June to August for about 15×10^{15} to 20×10^{15} molec·cm^{-2}, the low-VCD appeared in January to February and November to December for about 3×10^{15} to 9×10^{15} molec·cm^{-2}, and VCDs were comparable in remaining months (Fig. 1b). In addition, the amplitude of monthly HCHO VCDs was relatively smaller in 2018 and 2019, and mainly concentrated from 6×10^{15} to 15×10^{15} molec·cm^{-2}. The HCHO VCDs varied with the season, the maxima and minima corresponding to the respective summer and winter (Fig. 1c). Previous MAX-DOAS and OMI observations also exhibited the same seasonal patterns of HCHO in the YRD, China (Jin and Holloway, 2015; Chan et al., 2019). High temperature and abundant radiation are conducive to the plant growth to produce BVOCs and the photochemical reaction of VOCs, which boost the HCHO formation in summer (Sharkey and Loreto, 1993; Duncan et al., 2009; Narumi et al., 2009). Thus, HCHO VCDs would be relatively low in winter under the opposite weather conditions.

https://doi.org/10.5194/acp-2020-1298
Preprint. Discussion started: 25 February 2021

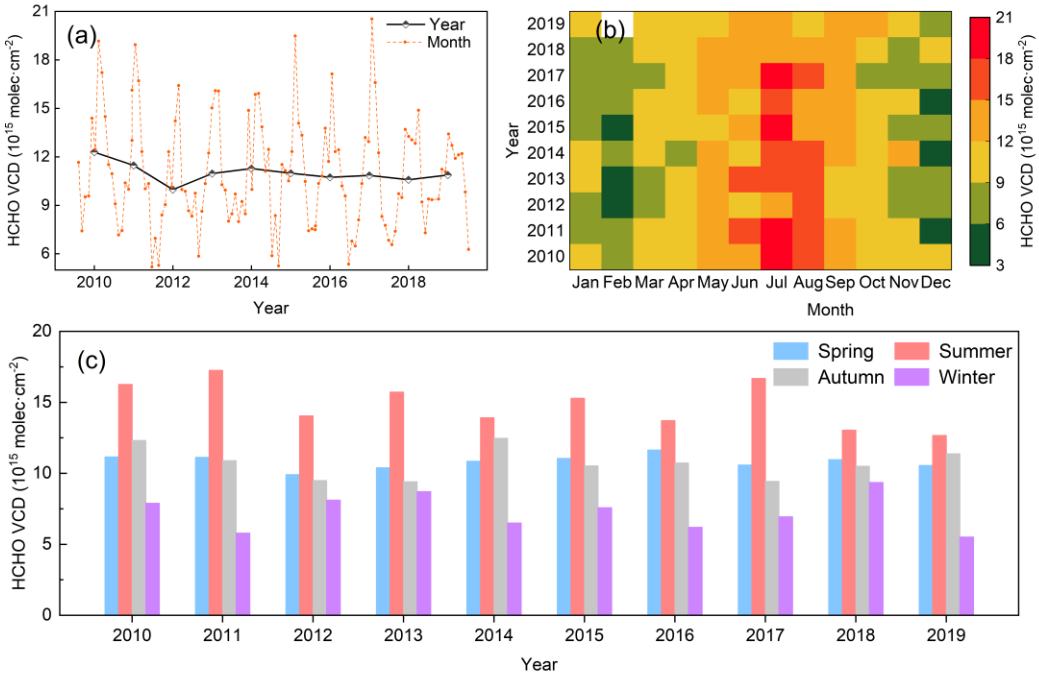

Figure 1. OMI observed time series of HCHO VCDs for (a) annual, (b) monthly and (c) seasonal variations in Shanghai during 2010-2019.

The spatial distribution of 10-year averaged HCHO VCD was given in Fig. 2a. In general, HCHO VCDs in eastern coastal area were relatively low, with the level of about 10×10^{15} molec·cm^{-2}. While those in western regions adjacent to other provinces were relatively higher, about 13×10^{15} molec·cm^{-2}. Noted that area with the highest HCHO VCD in Shanghai not appeared in the city center (marked by the red box) but in the relatively remote Qingpu (QP) district, followed by Songjiang (SJ) and Jinshan (JS) district. Figure 2b shows the difference of HCHO VCDs between 2019 and 2010. It suggests that except for the eastern and southern coastal areas, as well as the eastern area of Chongming Island, HCHO VCDs in Shanghai showed an overall downward trend during the past 10 years, with Qingpu district experiencing the largest decline. Figure 2c to Fig. 2f display the spatial distribution of HCHO VCDs in different seasons. HCHO VCD in summer was basically above 12×10^{15} molec·cm^{-2}. In winter, the value was around 7×10^{15} molec·cm^{-2} for most regions except for Qingpu district. While in spring and autumn, it was in the moderate level of about 10×10^{15} molec·cm^{-2}. The spatial distribution of HCHO VCDs in different seasons was similar to the 10-year averaged characteristics of high-value in the west and low-value in the east.

https://doi.org/10.5194/acp-2020-1298
Preprint. Discussion started: 25 February 2021

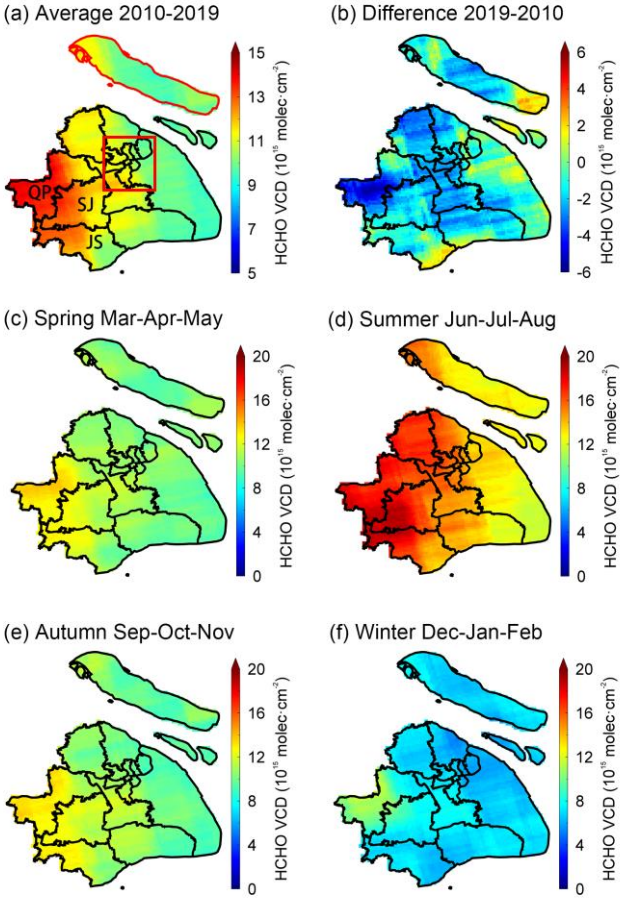

Figure 2. Spatial distribution of HCHO VCDs in Shanghai: (a) average HCHO VCD for 10 years, (b) the difference of HCHO VCDs between 2019 and 2010 (2019 minus 2010), and (c) to (f) for different seasons. In Fig. 2a the city center is marked with red box, Chongming Island is displayed with red boundary, QP, SJ, and JS refer to Qingpu, Songjiang, and Jinshan district.

3.2. Influencing factors

Figure 3 shows the monthly averaged HCHO VCDs and meteorological parameters, including temperature, sunshine hours, precipitation, and relative humidity from 2010 to 2018. Among these four meteorological factors, temperature had the most significant correlation with HCHO VCDs. Considering the daily averaged temperature was used here while HCHO VCDs observed by satellite only reflect the level at 13:45, the correlation between HCHO VCDs and temperature at 14:00 was further analysed, which demonstrated that the strong Pearson correlation coefficient is 0.842 at 0.01 level. It can be inferred that temperature is an important influencing factor of HCHO. The variation of sunshine hours from January to May was similar to that of HCHO VCDs. The reason for the positive effect of temperature and sunshine hours on HCHO VCDs is same as that mentioned in seasonal characteristics. It also implies indirectly the role of biogenic emissions in HCHO, which is favored by the high temperature and sunshine hours (Millet et al., 2008; Duncan et al., 2009). The precipitation and

https://doi.org/10.5194/acp-2020-1298
Preprint. Discussion started: 25 February 2021

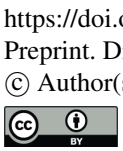

Atmospheric Chemistry and Physics Discussions

150 relative humidity reached peak in June, while the sunshine hours reached the dip. Abundant precipitation largely favoured the wet deposition of HCHO and offset the impact of rising temperature, resulting in a small decrease in HCHO VCDs in June (Pang et al., 2009).

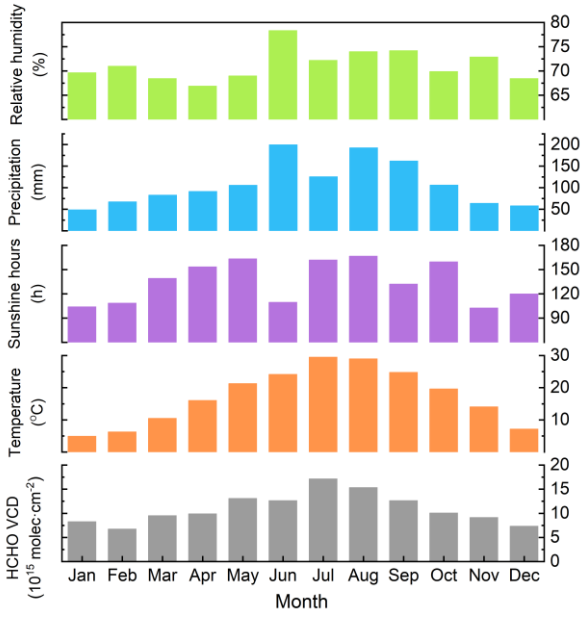

Figure 3. HCHO VCDs and meteorological factors including temperature, sunshine hours, precipitation and relative humidity in
155 **Shanghai for 2010-2018.**

To explore the impacts of anthropogenic sources on HCHO abundance, MEIC v.1.3 grid inventories for the year of 2010, 2012, 2014, and 2016 were used. HCHO emission inventory was calculated by the SAPRC07 chemical mechanism and MEIC VOCs inventory for different sectors of traffic, industrial, power and residential over these years. The emission of industrial sector was much higher than other sectors, accounting for about 87.9% of the total, followed by transportation
160 sector, accounting for about 10.8% (Fig. 4). Residential and power sectors were far lower, the proportion over these years was less than 1%. As major sectors, emission of industrial and transportation decreased about 30.9% and 58.5% respectively. In addition, the total anthropogenic emission of HCHO dropped 34.2% in 2016 compared with that in 2010, which was basically consistent with the total decrease in HCHO VCDs. It indicates that strengthening the control of industry and transportation should be an effective tactic for alleviating HCHO pollution.

https://doi.org/10.5194/acp-2020-1298
Preprint. Discussion started: 25 February 2021

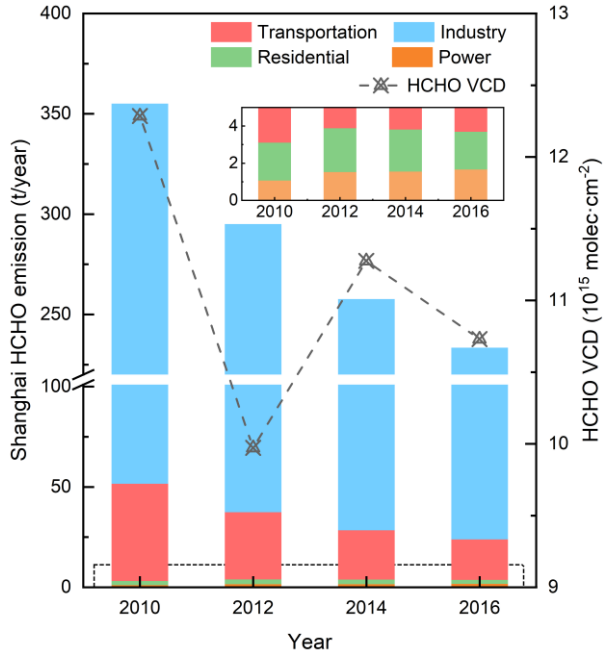

Figure 4. The variation of HCHO emission from anthropogenic sources including transportation, power, residential and industrial sectors.

3.3. FNR and O_3 formation regime

As the important precursors of O_3, HCHO and NO_2 can be served as indicators for VOCs and NO_x. On this basis, the HCHO/NO_2 ratio from satellite observation (FNR_{SAT}) can be employed to identify the O_3 formation regime. The variations of monthly averaged VCDs of HCHO, NO_2, and FNR_{SAT} in Shanghai over the past 10 years are given in Fig. 5. NO_2 VCDs were featured by the highest in winter and the lowest in summer, which was opposite to HCHO and fluctuated more fiercely. The peaks were mainly on account of its longer lifetime in winter (Zhang et al., 2007). While in summer, the adequate sunlight and precipitation accelerated the photochemical removal and wet deposition of NO_2, resulting in the dip (Wang et al., 2018; Xue et al., 2020). FNR_{SAT} also exhibited the obvious annual cycle of high in summer and low in winter. According to the criteria proposed by Duncan et.al (2010), O_3 formation regime in Shanghai was usually under NO_x-limited from June to August, and controlled by VOC-limited and transition regime for the rest of months. From May to September in 2014, Shanghai all under NO_x-limited regime, and FNR_{SAT} reached the highest value over the past 10 years. In 2019, the value of monthly FNR_{SAT} fluctuated gently, which showed the trend moving towards the transition regime threshold of 1-2.

https://doi.org/10.5194/acp-2020-1298
Preprint. Discussion started: 25 February 2021

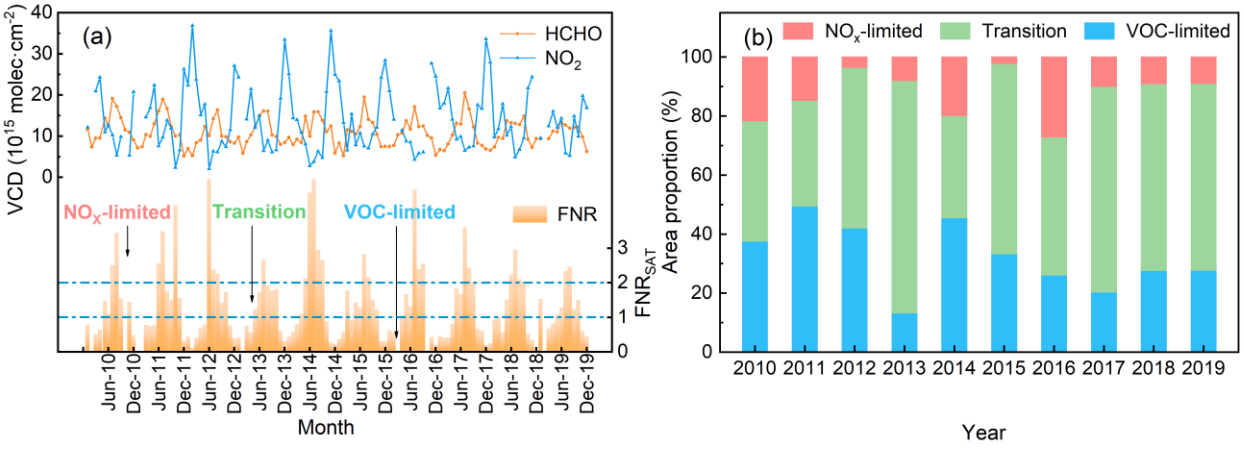

Figure 5. Temporal and spatial variation of FNR_{SAT} in Shanghai: (a) variations of HCHO, NO_2 and FNR_{SAT} from 2010 to 2019, and (b) the area proportion for different O_3 formation regimes in these years.

The spatial distribution of FNR_{SAT} in Shanghai is presented in Fig. 6. Comparing FNR_{SAT} in 2019 with that in 2010, the NO_x-limited regime in the western Shanghai transformed into transition regime, and VOC-limited regime in the northern Chongming Island almost completely became transition regime. It manifests itself in the reduction in the NO_x-limited and VOC-limited regimes while the increase in the transition regime. Referring to previous study on the variation of NO_2 VCDs spatial distribution in Shanghai observed by satellite, this phenomenon may be related to the spatial characteristics of concentration variations of two precursors (Xue et al., 2020). This result is also reflected in Fig. 5b. In the past 10 years, the proportion decreased from 37.6% to 27.7% for VOC-limited area, and from 21.6% to 8.9% for NO_x-limited area, respectively. Meanwhile, the transition regime area increased from 40.8% to 63.3%. Xu et al. (2019) suggested that O_3 formation regime in Shanghai trend to transform from VOC-limited regime to NO_x-limited regime after 2020 through WRF-Chem model simulation. In this study, the increase of transition regime may be the transition state from VOC-limited to NO_x-limited regime.

https://doi.org/10.5194/acp-2020-1298
Preprint. Discussion started: 25 February 2021

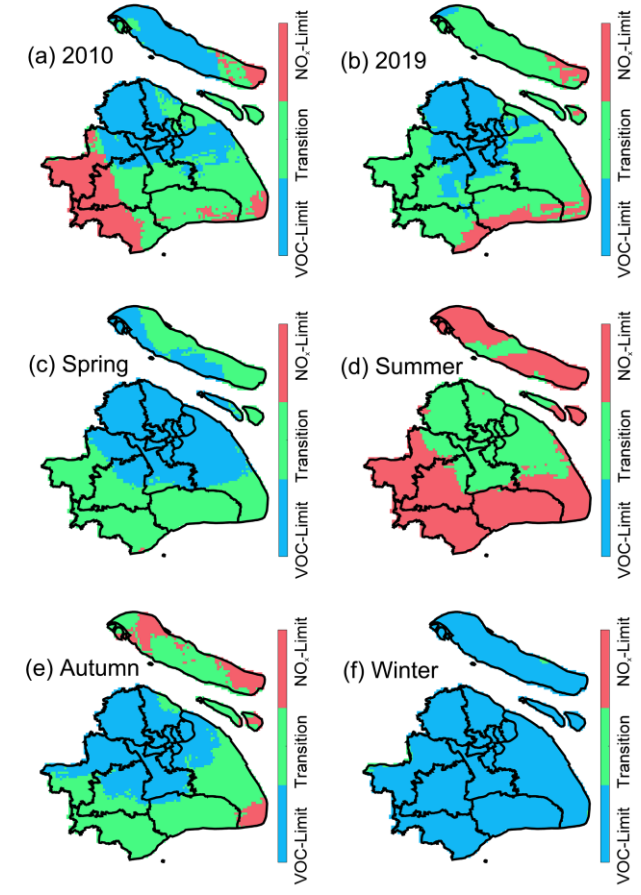

Figure 6. The spatial distribution of FNR_{SAT} for (a) 2010, (b) 2019, and (c) to (f) different seasons in Shanghai.

Figure. 6c to Fig. 6f show the spatial distribution of FNR_{SAT} for different seasons during the decade. In spring, the northern area of Shanghai was VOC-limited regime while the southern area was transition regime. From spring to summer, the VOC-limited area almost transformed into transition regime, and the transition regime nearly turned into NO_x-limited at the same time, which mainly caused by the increase of HCHO and the decrease of NO_2. The distribution in autumn was similar to that in spring. In winter, Shanghai was basically under VOC-limited. In the light of the temporal and spatial distribution of O_3 formation regime inferred by FNR_{SAT}, the emission reduction measures for O_3 precursors would be more rationally.

Besides, there are differences in O_3 formation regime in urban and rural areas of Shanghai, with the main manifestation that the central urban area was inclined to be in VOC-limited regime and the rural area was more likely to be in NO_x-limited regime. In order to analyse the differences in more detail, area within 10 km around the Jiangwan campus of Fudan University was selected to represent the urban area, and equally sized area around Dianshan Lake (31.09°N, 120.98°E) of Qingpu district was regarded as the rural area, respectively. Since O_3 pollution is relatively serious from April to September, this period can be chosen as a research case. The maximum 8-hour average concentration of O_3 at the Hongkou and the Qingpu Dianshan Lake Site were used to characterize O_3 concentration in urban and rural areas. NO_2 VCDs in urban area

https://doi.org/10.5194/acp-2020-1298
Preprint. Discussion started: 25 February 2021

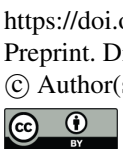

Atmospheric Chemistry and Physics Discussions

were higher than that in rural, while HCHO VCDs presented the opposite character (Fig. 7a). The lower NO_2 in rural area was associated with the less NO_x emission than that in urban, corresponding to the larger FNR_{SAT}. From Fig. 7b, the O_3 production was under transition regime in rural area except for 2016, while VOC-limited regime occupied for most years in urban area. The O_3 concentration in rural area was always higher than that in urban (Fig. 7c). In this study, transition regime in rural for most years led to higher O_3 concentration correspondingly (Jin et al., 2020). In addition, high concentration of NO_x in urban area may lead to titration of O_3 by NO, which would also cause the lower O_3 concentration in urban (Geng et al., 2008; Duncan et al., 2010).

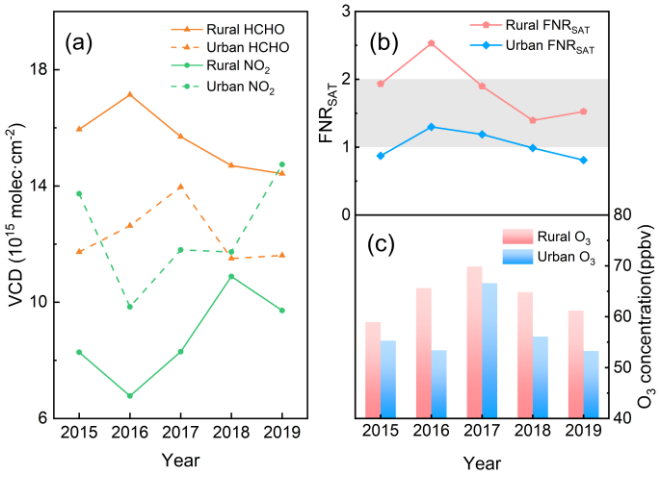

Figure 7. Differences of (a) satellite observation of HCHO and NO_2 VCDs, (b) FNR_{SAT} and (c) surface O_3 concentration in urban and rural areas of Shanghai from 2015 to 2019.

3.4. Correction of FNR_{SAT}

FNR is originally proposed as an indicator to characterize the sensitivity of the instantaneous O_3 production rate (Duncan et al., 2010). Satellite observation only reflects the averaged column of the trace gases around overpass time, so the FNR_{SAT} may not accurately infer the surface O_3 formation regime during the day (Duncan et al., 2010; Jin and Holloway, 2015; Jin et al., 2017). LP-DOAS observation provides surface concentration of O_3 precursors with the high temporal resolution throughout the day, therefore FNR observed by LP-DOAS (FNR_{LP}) should be more suitable for distinguishing the formation regime of surface O_3. Here FNR_{SAT} and FNR_{LP} were compared together as the function of surface O_3 concentration. Only FNR_{LP} from 08:00 to 18:00 LT were considered owing to the relatively strong photochemical reaction of O_3 formation for this period. FNR_{SAT} was spatially averaged for grids within 10 km of the LP-DOAS measurement site. Then, three cases were selected for the further discussion under the criteria of the hourly concentration of O_3 exceeding 200 μg/m^3 (secondary concentration limit stipulated in ambient air quality standards of China, GB 3095-2012).

In Fig. 8a and Fig. 8c, the upward trend in FNR_{LP} as the O_3 concentration increases means that the formation of O_3 was under VOC-limited regime in Case 1 and 3. VOC-limited and transition regimes caught in Case 1 through FNR_{SAT} were different from that identified by FNR_{LP}. In Case 3, the O_3 formation regime remained in VOC-limited regime, which was the

https://doi.org/10.5194/acp-2020-1298
Preprint. Discussion started: 25 February 2021

Atmospheric Chemistry and Physics Discussions

same as FNR_{LP}. As shown in Fig. 8b, FNR_{LP} indicated that the O_3 formation regime switched between three regimes in Case 2. As O_3 concentration increasing, the growth of FNR_{LP} at beginning indicated VOC-limited regime, while the subsequent slow variation suggested transition regime. When O_3 concentration reached maximum, FNR_{LP} got smaller, which referred to NO_x-limited regime. But FNR_{SAT} only captured the VOC-limited and transition regime in Case 2. According to the results above, it is feasible and necessary to correct FNR_{SAT} to better represent the sensitivity of surface O_3 formation. Due to the less O_3 pollution in winter, FNR_{SAT} was only corrected for the remaining three seasons.

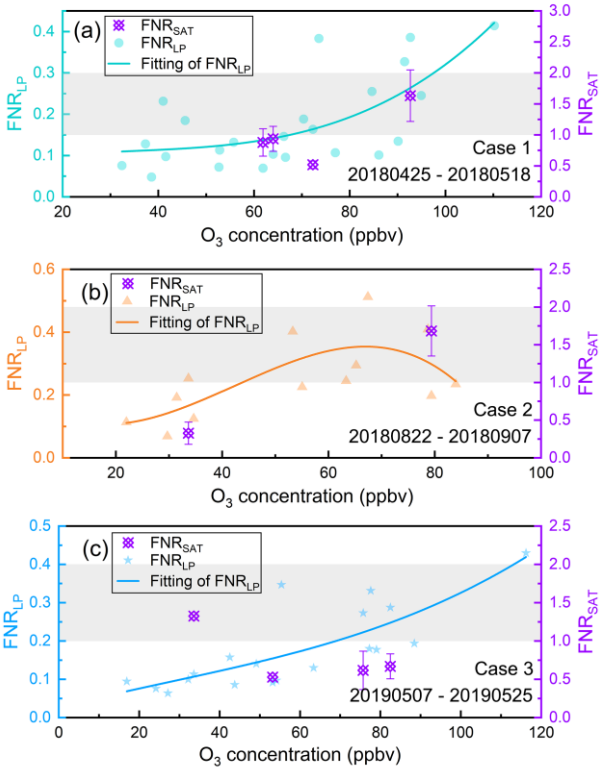

Figure 8. Comparison of FNR_{SAT} and FNR_{LP} in three O_3 pollution cases. The curves are polynomial fit of FNR_{LP}, and the points are FNR_{SAT} in corresponding cases, the gray area indicates the transition regime for FNR_{SAT}.

As shown in Fig. 9a, the highest value of FNR_{LP} at noon means that FNR_{SAT} at overpass time approximately close to the highest level in a day. Therefore, we consider to utilize the ground surface FNR diurnal pattern observed by LP-DOAS during ozone polluted period to correct the FNR_{SAT}. It is noted that the ozone polluted period was defined as the duration with positive increment of hourly O_3 concentration, as referred to Eq. (3) and Fig. 9b, where can be seen that the ΔO_3 greater than 0 from 07:00 to 13:00 LT.

Firstly, the ratio of FNR at satellite overpass time to averaged FNR during O_3 pollution period obtained from ground surface measurement was assumed to be same with that of satellite observation, which is expressed as:

$$\frac{FNR_{SAT}}{FNR_{SAT}} = \frac{FNR_{LP,overpass\ time}}{FNR_{LP}} \quad (1)$$

https://doi.org/10.5194/acp-2020-1298
Preprint. Discussion started: 25 February 2021

Atmospheric Chemistry and Physics Discussions

where $\overline{FNR}_{LP}$ is weighted average of FNR during O_3 pollution period observed by ground surface LP-DOAS measurement, $FNR_{LP,overpass\ time}$ is ground surface FNR observed at satellite overpass time. $\frac{FNR_{LP,overpass\ time}}{\overline{FNR}_{LP}}$ reflects the numerical relationship of FNR between satellite overpassed time and O_3 polluted period during a day, and can be serve as the correction coefficient to realize the correction for FNR_{SAT} on time scale to obtain the $\overline{FNR}_{SAT}$. Considering the relationship between FNR and O_3 formation, ΔO_3 was involved to calculate the weighted average of FNR_{LP} ($\overline{FNR}_{LP}$) during 07:00 to 13:00 LT via Eq. (2), which can better indicate the ozone formation in a day.

$$\overline{FNR}_{LP} = \frac{\sum_{T=7}^{13} FNR_{LP,T} \times \Delta\Omega_{O3,T}}{\sum_{T=7}^{13} \Delta\Omega_{O3,T}} \quad (2)$$

$$\Delta\Omega_{O3,T} = \Omega_{O3,T} - \Omega_{O3,T-1} \quad (3)$$

Where $\Delta\Omega_{O3,T}$ is the increase of O_3 concentration at time T, $FNR_{LP,T}$ is the FNR_{LP} at time T. Moreover, variation characteristics of FNR_{LP} in different seasons suggest that the correction of FNR_{SAT} should be discussed seasonally.

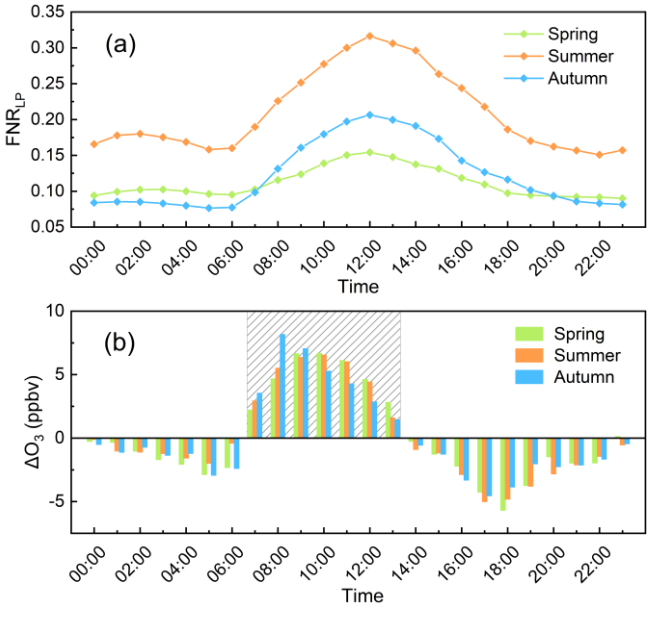

Figure 9. Diurnal variations of (a) FNR_{LP} and (b) ΔO_3 for different seasons in 2018-2019. The shaded area represents the period when ΔO_3 greater than 0.

Afterwards, the seasonal correction coefficients of 0.85, 0.84, and 0.77 were obtained for spring, summer, and autumn, respectively. It is noted that all the correct coefficients were less than 1 due to the FNR_{LP} value for OMI overpasses time relatively larger than other time. It would inevitably make the O_3 formation regime inferred by corrected FNR_{SAT} trend to be VOC-limited. There were 87 months with effective FNR_{SAT} in three seasons during 2010-2019 and the proportion of months for different regimes was listed in Table 1. Before the correction, the VOC-limited and NO_x-limited regimes, as well as transition regime were almost accounted for about one-third of the total months. After the correction, both of months for

https://doi.org/10.5194/acp-2020-1298
Preprint. Discussion started: 25 February 2021

Atmospheric Chemistry and Physics Discussions

VOC-limited and transition regimes increased. The months under VOC-limited regime increased by 25% particularly, while decreased about 32.1% for NO_x-limited regime. Jin et al. (2020) used O_3 exceedance probability as the indicator to analyse non-linear dependence of long-term surface O_3 concentration on precursor emissions, and determined the OMI $HCHO/NO_2$ under transition regime ranging from 3.2 to 4.1. These thresholds are significantly larger than the value proposed by Duncan et al. (2010), which has the equivalent effect as the use of correction factors less than 1 in this study.

Table 1. Variations in the number and proportions of months in 2010-2019 for each regime before and after the correction.

Regime	Before corrected	Percentage before corrected	After corrected	Percentage after corrected	Percentage of change
VOC-limited	28	32.2%	35	40.2%	25.0%
Transition	31	35.6%	33	37.9%	6.5%
NO_x-limited	28	32.2%	19	21.8%	-32.1%

In terms of spatial distribution, the O_3 formation regime after correction in different seasons is shown in Fig. 10. Compared with Fig. 6, part of the transition regime area in spring transformed into VOC-limited regime after the correction, VOC-limited regime obviously expanded and increased about 15.6%. Most area in Chongming Island transformed into VOC-limited regime. In summer, part of the NO_x-limited regime area transformed into transition regime, and the area of transition regime increased about 11.9%. In autumn, the NO_x-limited regime almost disappeared, and the proportion of the transition regime area also decreased significantly, for about 13.2%, while the proportion of the VOC-limited regime area increased about 22%. The O_3 formation regime in Chongming Island was basically under transition regime. Researchers also pointed that thresholds of criteria would be regionally dependent, so the local surface FNR and O_3 concentration should be introduced in satellite correction (Duncan et al., 2010; Jin et al., 2020).

https://doi.org/10.5194/acp-2020-1298
Preprint. Discussion started: 25 February 2021

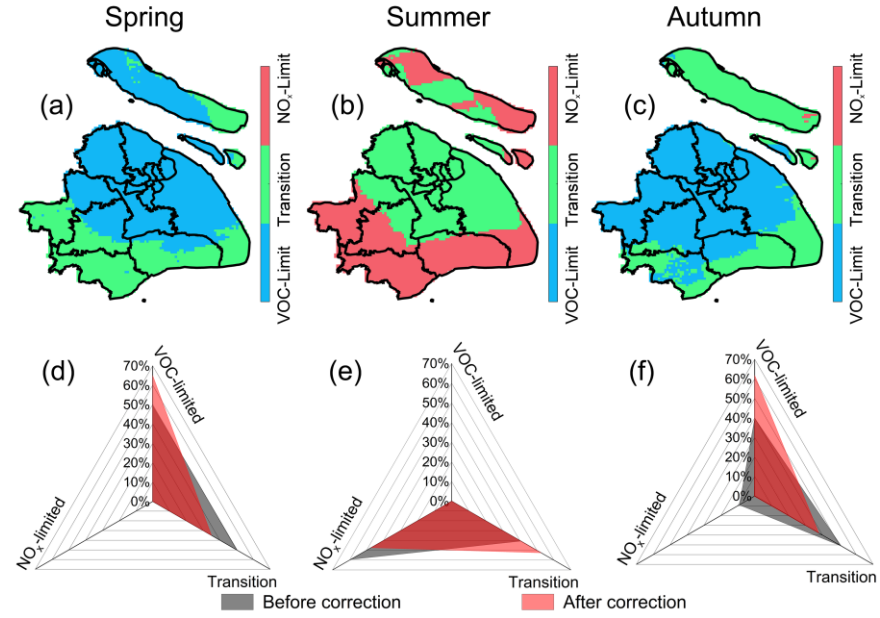

Figure 10. Spatial distribution of O_3 formation regime (upper row) and area proportion for each regime (bottom row) after correction for different seasons in Shanghai during 2010-2019.

The O_3 formation regimes before and after the correction were compared with regime inferred by FNR_{LP} in Fig. 11. It can be seen from Fig. 9a that FNR_{LP} is significantly lower than 1, and it is not suitable for the threshold of FNR_{SAT} method to infer the O_3 formation regime. To infer the influence of precursors on O_3, linear regression was executed for precursors observed by LP-DOAS and O_3 concentration. O_3 formation regime was discerned by comparing the slopes versus HCHO and NO_2 (O_3-HCHO and O_3-NO_2: both positive reflect transition regime; positive and negative means VOC-limited; negative and positive suggests NO_x-limited; both negative indicates titration of O_3 by NO and classified as VOC-limited) (Su et al., 2017; Chi et al., 2018). In several months, LP-DOAS observation indicated VOC-limited or transition regime, while the FNR_{SAT} reflected transition or NO_x-limited regime, which mainly related to the high level of FNR at the overpass time of OMI. After the correction, the result of satellite was closer to LP-DOAS obviously, indicating that the correction of FNR_{SAT} in this study is effective.

https://doi.org/10.5194/acp-2020-1298
Preprint. Discussion started: 25 February 2021

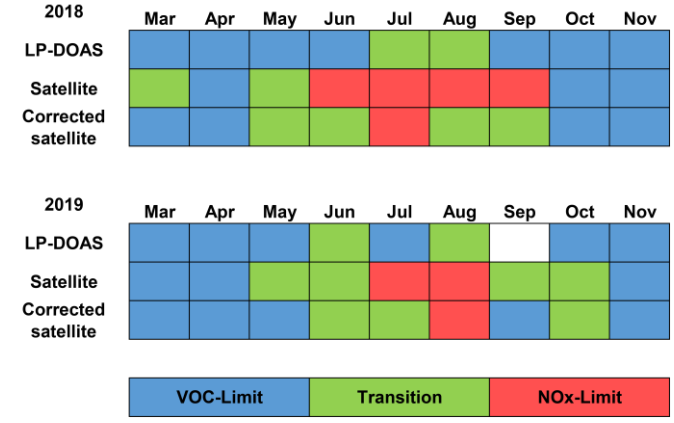

Figure 11. The comparison of the observation results of the FNR_{SAT} and LP-DOAS on the O_3 formation regime in Shanghai 2018-2019 for each month except for winter. In each year, the top row represents the LP-DOAS observation result, the middle row represents the FNR_{SAT} observation before correction, and the bottom row represents the FNR_{SAT} observation after the correction.

4. Summary and conclusions

Satellite data of OMI were used to study the temporal and spatial variation of HCHO in Shanghai from 2010 to 2019. HCHO VCDs fluctuated during the 10 years with obvious seasonal characteristics of highest value in summer, the lowest value in winter, and the moderate level in spring and autumn. In terms of spatial distribution, HCHO VCDs in western area were much higher than that in eastern coastal area. Compared with 2010, HCHO VCDs of Shanghai in 2019 showed an overall downward trend. As for the influencing factors, temperature and sunlight give the significant positive effect on HCHO VCDs while the abundant precipitation reduce HCHO in atmosphere. Industry was an important emission sector of HCHO, similarly showing a downward trend due to the government control.

In the past 10 years, O_3 formation regime changed toward transition regime gradually. O_3 formation regime in urban area was more likely to be VOC-limited regime, while regime in rural area was more likely to be NO_x-limited. FNR_{SAT} was corrected based on the hourly surface FNR and O_3 data to make it better to reflect O_3 formation in a day. After correcting FNR_{SAT} with seasonal correction coefficients of 0.85, 0.84, and 0.77 for spring, summer, and autumn respectively, O_3 formation regime in Shanghai was more inclined to VOC-limited in both time and spatial distribution, and was closer to the observation result of LP-DOAS. Thus, this correction is significant for using satellite data to improve the accuracy in indicating surface O_3 formation.

Data availability. Data are available for scientific purposes upon request to the corresponding author.

Author Contributions: DL and SW designed and implemented the research, and prepared the manuscript; RX contributed to the analysis of OMI products and MEIC inventory; JZ provided the HCHO and NO_2 data observed by LP-DOAS; SZ and ZS revised the manuscript; BZ provided constructive comments and supported the DOAS measurements.

https://doi.org/10.5194/acp-2020-1298
Preprint. Discussion started: 25 February 2021

Atmospheric Chemistry and Physics Discussions

Competing interests. The authors declare that they have no conflict of interest.

Acknowledgments: We acknowledge the free use of OMI HCHO and NO_2 products from NASA Goddard Earth Sciences (GES) Data and Information Services Center (DISC). We also thank Center for Earth System Science, Tsinghua University for MEIC data.

Financial support: This research was funded by National Key Research and Development Program of China (2017YFC0210002), National Natural Science Foundation of China (41775113, 21777026).

References

Bovensmann, H., Burrows, J. P., Buchwitz, M., Frerick, J., Noel, S., Rozanov, V. V., Chance, K. V., and Goede, A. P. H.: SCIAMACHY: Mission objectives and measurement modes, J Atmos Sci, 56, 127-150, https://doi.org/Doi 10.1175/1520-0469(1999)056<0127:Smoamm>2.0.Co;2, 1999.

Burrows, J. P., Weber, M., Buchwitz, M., Rozanov, V., Ladstatter-Weissenmayer, A., Richter, A., DeBeek, R., Hoogen, R., Bramstedt, K., Eichmann, K. U., and Eisinger, M.: The global ozone monitoring experiment (GOME): Mission concept and first scientific results, J Atmos Sci, 56, 151-175, https://doi.org/Doi 10.1175/1520-0469(1999)056<0151:Tgomeg>2.0.Co;2, 1999.

Callies, J., Corpaccioli, E., Eisinger, M., Hahne, A., and Lefebvre, A.: GOME-2 - Metop's second-generation sensor for operational ozone monitoring, Esa Bull-Eur Space, 28-36, 2000.

Chan, K. L., Wang, Z. R., Ding, A. J., Heue, K. P., Shen, Y. C., Wang, J., Zhang, F., Shi, Y. N., Hao, N., and Wenig, M.: MAX-DOAS measurements of tropospheric NO_2 and HCHO in Nanjing and a comparison to ozone monitoring instrument observations, Atmos Chem Phys, 19, 10051-10071, https://doi.org/10.5194/acp-19-10051-2019, 2019.

Chi, X. Y., Liu, C., Xie, Z. Q., Fan, G. Q., Wang, Y., He, P. Z., Fan, S. D., Hong, Q. Q., Wang, Z., Yu, X. W., Yue, F. E., Duan, J. B., Zhang, P. F., and Liu, J. G.: Observations of ozone vertical profiles and corresponding precursors in the low troposphere in Beijing, China, Atmos Res, 213, 224-235, https://doi.org/10.1016/j.atmosres.2018.06.012, 2018.

De Smedt, I., Van Roozendael, M., Stavrakou, T., Muller, J. F., Lerot, C., Theys, N., Valks, P., Hao, N., and van der A, R.: Improved retrieval of global tropospheric formaldehyde columns from GOME-2/MetOp-A addressing noise reduction and instrumental degradation issues, Atmos Meas Tech, 5, 2933-2949, https://doi.org/10.5194/amt-5-2933-2012, 2012.

Duncan, B. N., Yoshida, Y., Damon, M. R., Douglass, A. R., and Witte, J. C.: Temperature dependence of factors controlling isoprene emissions, Geophys Res Lett, 36, https://doi.org/10.1029/2008GL037090, 2009.

Duncan, B. N., Yoshida, Y., Olson, J. R., Sillman, S., Martin, R. V., Lamsal, L., Hu, Y. T., Pickering, K. E., Retscher, C., Allen, D. J., and Crawford, J. H.: Application of OMI observations to a space-based indicator of NO_x and VOC controls on surface ozone formation, Atmos Environ, 44, 2213-2223, https://doi.org/10.1016/j.atmosenv.2010.03.010, 2010.

Geng, F. H., Tie, X. X., Xu, J. M., Zhou, G. Q., Peng, L., Gao, W., Tang, X., and Zhao, C. S.: Characterizations of ozone, NO_x, and VOCs measured in Shanghai, China, Atmos Environ, 42, 6873-6883, https://doi.org/10.1016/j.atmosenv.2008.05.045, 2008.

Jin, X. M., and Holloway, T.: Spatial and temporal variability of ozone sensitivity over China observed from the Ozone Monitoring Instrument, J. Geophys. Res.-Atmos., 120, 7229-7246, https://doi.org/10.1002/2015jd023250, 2015.

Jin, X. M., Fiore, A. M., Murray, L. T., Valin, L. C., Lamsal, L. N., Duncan, B., Folkert Boersma, K., De Smedt, I., Abad, G. G., Chance, K., and Tonnesen, G. S.: Evaluating a Space-Based Indicator of Surface Ozone-NO_x-VOC Sensitivity Over Midlatitude Source Regions and Application to Decadal Trends, J. Geophys. Res.-Atmos., 122, 10231-10253, https://doi.org/10.1002/2017jd026720, 2017.

https://doi.org/10.5194/acp-2020-1298
Preprint. Discussion started: 25 February 2021

Atmospheric Chemistry and Physics Discussions

Jin, X. M., Fiore, A., Boersma, K. F., De Smedt, I., and Valin, L.: Inferring Changes in Summertime Surface Ozone-NO_x-VOC Chemistry over US Urban Areas from Two Decades of Satellite and Ground-Based Observations, Environ Sci Technol, 54, 6518-6529, https://doi.org/10.1021/acs.est.9b07785, 2020.

Krotkov, N. A., McLinden, C. A., Li, C., Lamsal, L. N., Celarier, E. A., Marchenko, S. V., Swartz, W. H., Bucsela, E. J., Joiner, J., Duncan, B. N., Boersma, K. F., Veefkind, J. P., Levelt, P. F., Fioletov, V. E., Dickerson, R. R., He, H., Lu, Z. F., and Streets, D. G.: Aura OMI observations of regional SO_2 and NO_2 pollution changes from 2005 to 2015, Atmos Chem Phys, 16, 4605-4629, https://doi.org/10.5194/acp-16-4605-2016, 2016.

Lee, H., Ryu, J., Irie, H., Jang, S. H., Park, J., Choi, W., and Hong, H.: Investigations of the Diurnal Variation of Vertical HCHO Profiles Based on MAX-DOAS Measurements in Beijing: Comparisons with OMI Vertical Column Data, Atmosphere-Basel, 6, 1816-1832, https://doi.org/10.3390/atmos6111816, 2015.

Levelt, P. F., Van den Oord, G. H. J., Dobber, M. R., Malkki, A., Visser, H., de Vries, J., Stammes, P., Lundell, J. O. V., and Saari, H.: The Ozone Monitoring Instrument, Ieee T Geosci Remote, 44, 1093-1101, https://doi.org/10.1109/Tgrs.2006.872333, 2006.

Li, X., Rohrer, F., Brauers, T., Hofzumahaus, A., Lu, K., Shao, M., Zhang, Y. H., and Wahner, A.: Modeling of HCHO and CHOCHO at a semi-rural site in southern China during the PRIDE-PRD2006 campaign, Atmos Chem Phys, 14, 12291-12305, https://doi.org/10.5194/acp-14-12291-2014, 2014.

Ling, Z. H., Guo, H., Chen, G. X., Lam, S. H. M., and Fan, S. J.: Formaldehyde and Acetaldehyde at Different Elevations in Mountainous Areas in Hong Kong, Aerosol Air Qual Res, 16, 1868-1878, https://doi.org/10.4209/aaqr.2015.09.0571, 2016.

Liu, H. R., Liu, C., Xie, Z. Q., Li, Y., Huang, X., Wang, S. S., Xu, J., and Xie, P. H.: A paradox for air pollution controlling in China revealed by "APEC Blue" and "Parade Blue", Sci Rep-Uk, 6, 13, https://doi.org/10.1038/srep34408, 2016.

Liu, R., Feng, T., Wang, S. S., Shi, C. Z., Guo, Y. L., Nan, J. L., Deng, Y., and Zhou, B.: OMI satellite observed formaldehyde column from 2006 to 2015 over Xishuangbanna, southwest China, and validation using ground based zenith-sky DOAS, Sci Total Environ, 613, 168-175, https://doi.org/10.1016/j.scitotenv.2017.08.210, 2018.

Liu, Y., Tang, Z. P., Abera, T., Zhang, X. Z., Hakola, H., Pellikka, P., and Maeda, E.: Spatio-temporal distribution and source partitioning of formaldehyde over Ethiopia and Kenya, Atmos Environ, 237, 9, https://doi.org/10.1016/j.atmosenv.2020.117706, 2020.

Martin, R. V., Fiore, A. M., and Van Donkelaar, A.: Space-based diagnosis of surface ozone sensitivity to anthropogenic emissions, Geophys Res Lett, 31, L06120 06121-06124, https://doi.org/10.1029/2004gl019416, 2004a.

Martin, R. V., Parrish, D. D., Ryerson, T. B., Nicks, D. K., Chance, K., Kurosu, T. P., Jacob, D. J., Sturges, E. D., Fried, A., and Wert, B. P.: Evaluation of GOME satellite measurements of tropospheric NO_2 and HCHO using regional data from aircraft campaigns in the southeastern United States, J. Geophys. Res.-Atmos., 109, 11, https://doi.org/10.1029/2004jd004869, 2004b.

Millet, D. B., Jacob, D. J., Boersma, K. F., Fu, T. M., Kurosu, T. P., Chance, K., Heald, C. L., and Guenther, A.: Spatial distribution of isoprene emissions from North America derived from formaldehyde column measurements by the OMI satellite sensor, J. Geophys. Res.-Atmos., 113, 18, https://doi.org/10.1029/2007jd008950, 2008.

Narumi, D., Kondo, A., and Shimoda, Y.: The effect of the increase in urban temperature on the concentration of photochemical oxidants, Atmos Environ, 43, 2348-2359, https://doi.org/10.1016/j.atmosenv.2009.01.028, 2009.

Pang, X. B., Mu, Y. J., Lee, X. Q., Zhang, Y. J., and Xu, Z.: Influences of characteristic meteorological conditions on atmospheric carbonyls in Beijing, China, Atmos Res, 93, 913-919, https://doi.org/10.1016/j.atmosres.2009.05.001, 2009.

Schroeder, J. R., Crawford, J. H., Fried, A., Walega, J., Weinheimer, A., Wisthaler, A., Muller, M., Mikoviny, T., Chen, G., Shook, M., Blake, D. R., and Tonnesen, G. S.: New insights into the column CH_2O/NO_2 ratio as an indicator of near-surface ozone sensitivity, J. Geophys. Res.-Atmos., 122, 8885-8907, https://doi.org/10.1002/2017jd026781, 2017.

Sharkey, T. D., and Loreto, F.: Water stress, temperature, and light effects on the capacity for isoprene emission and photosynthesis of kudzu leaves, Oecologia, 95, 328-333, https://doi.org/10.1007/bf00320984, 1993.

Shen, L., Jacob, D. J., Zhu, L., Zhang, Q., Zheng, B., Sulprizio, M. P., Li, K., De Smedt, I., Abad, G. G., Cao, H. S., Fu, T. M., and Liao, H.: The 2005-2016 Trends of Formaldehyde Columns Over China Observed by Satellites: Increasing Anthropogenic Emissions of Volatile Organic Compounds and Decreasing Agricultural Fire Emissions, Geophys Res Lett, 46, 4468-4475, https://doi.org/10.1029/2019gl082172, 2019.

https://doi.org/10.5194/acp-2020-1298
Preprint. Discussion started: 25 February 2021

Atmospheric Chemistry and Physics Discussions

Sillman, S.: The Use of Noy, H2o2, and Hno3 as Indicators for Ozone-Nox-Hydrocarbon Sensitivity in Urban Locations, J. Geophys. Res.-Atmos., 100, 14175-14188, https://doi.org/Doi 10.1029/94jd02953, 1995.

Souri, A. H., Choi, Y., Jeon, W., Woo, J. H., Zhang, Q., and Kurokawa, J.: Remote sensing evidence of decadal changes in major tropospheric ozone precursors over East Asia, J. Geophys. Res.-Atmos., 122, 2474-2492, https://doi.org/10.1002/2016jd025663, 2017.

Stavrakou, T., Muller, J. F., De Smedt, I., Van Roozendael, M., van der Werf, G. R., Giglio, L., and Guenther, A.: Global emissions of non-methane hydrocarbons deduced from SCIAMACHY formaldehyde columns through 2003-2006, Atmos Chem Phys, 9, 3663-3679, https://doi.org/10.5194/acp-9-3663-2009, 2009.

Su, W. J., Liu, C., Hu, Q. H., Fan, G. Q., Xie, Z. Q., Huang, X., Zhang, T. S., Chen, Z. Y., Dong, Y. S., Ji, X. G., Liu, H. R., Wang, Z., and Liu, J. G.: Characterization of ozone in the lower troposphere during the 2016 G20 conference in Hangzhou, Sci Rep-Uk, 7, 11, https://doi.org/10.1038/s41598-017-17646-x, 2017.

Su, W. J., Liu, C., Hu, Q. H., Zhao, S. H., Sun, Y. W., Wang, W., Zhu, Y. Z., Liu, J. G., and Kim, J.: Primary and secondary sources of ambient formaldehyde in the Yangtze River Delta based on Ozone Mapping and Profiler Suite (OMPS) observations, Atmos Chem Phys, 19, 6717-6736, https://doi.org/10.5194/acp-19-6717-2019, 2019.

Veefkind, J. P., Aben, I., McMullan, K., Forster, H., de Vries, J., Otter, G., Claas, J., Eskes, H. J., de Haan, J. F., Kleipool, Q., van Weele, M., Hasekamp, O., Hoogeveen, R., Landgraf, J., Snel, R., Tol, P., Ingmann, P., Voors, R., Kruizinga, B., Vink, R., Visser, H., and Levelt, P. F.: TROPOMI on the ESA Sentinel-5 Precursor: A GMES mission for global observations of the atmospheric composition for climate, air quality and ozone layer applications, Remote Sens Environ, 120, 70-83, https://doi.org/10.1016/j.rse.2011.09.027, 2012.

Vigouroux, C., Langerock, B., Aquino, C. A. B., Blumenstock, T., Cheng, Z. B., De Maziere, M., De Smedt, I., Grutter, M., Hannigan, J. W., Jones, N., Kivi, R., Loyola, D., Lutsch, E., Mahieu, E., Makarova, M., Metzger, J. M., Morino, I., Murata, I., Nagahama, T., Notholt, J., Ortega, I., Palm, M., Pinardi, G., Rohling, A., Smale, D., Stremme, W., Strong, K., Sussmann, R., Te, Y., van Roozendael, M., Wang, P. C., and Winkler, H.: TROPOMI-Sentinel-5 Precursor formaldehyde validation using an extensive network of ground-based Fourier-transform infrared stations, Atmos Meas Tech, 13, 3751-3767, https://doi.org/10.5194/amt-13-3751-2020, 2020.

Wang, T., Wang, P. C., Theys, N., Tong, D., Hendrick, F., Zhang, Q., and Van Roozendael, M.: Spatial and temporal changes in SO_2 regimes over China in the recent decade and the driving mechanism, Atmos Chem Phys, 18, 18063-18078, https://doi.org/10.5194/acp-18-18063-2018, 2018.

Wang, Y., Beirle, S., Lampel, J., Koukouli, M., De Smedt, I., Theys, N., Li, A., Wu, D. X., Xie, P. H., Liu, C., Van Roozendael, M., Stavrakou, T., Muller, J. F., and Wagner, T.: Validation of OMI, GOME-2A and GOME-2B tropospheric NO_2, SO_2 and HCHO products using MAX-DOAS observations from 2011 to 2014 in Wuxi, China: investigation of the effects of priori profiles and aerosols on the satellite products, Atmos Chem Phys, 17, 5007-5033, https://doi.org/10.5194/acp-17-5007-2017, 2017.

Xing, C. Z., Liu, C., Hu, Q. H., Fu, Q. Y., Lin, H., Wang, S. T., Su, W. J., Wang, W. W., Javed, Z., and Liu, J. G.: Identifying the wintertime sources of volatile organic compounds (VOCs) from MAX-DOAS measured formaldehyde and glyoxal in Chongqing, southwest China, Sci Total Environ, 715, 12, https://doi.org/10.1016/j.scitotenv.2019.136258, 2020.

Xu, J. M., Tie, X. X., Gao, W., Lin, Y. F., and Fu, Q. Y.: Measurement and model analyses of the ozone variation during 2006 to 2015 and its response to emission change in megacity Shanghai, China, Atmos Chem Phys, 19, 9017-9035, https://doi.org/10.5194/acp-19-9017-2019, 2019.

Xue, R. B., Wang, S. S., Li, D. R., Zou, Z., Chan, K. L., Valks, P., Saiz-Lopez, A., and Zhou, B.: Spatio-temporal variations in NO_2 and SO_2 over Shanghai and Chongming Eco-Island measured by Ozone Monitoring Instrument (OMI) during 2008-2017, J Clean Prod, 258, 14, https://doi.org/10.1016/j.jclepro.2020.120563, 2020.

Zaveri, R. A., Berkowitz, C. M., Kleinman, L. I., Springston, S. R., Doskey, P. V., Lonneman, W. A., and Spicer, C. W.: Ozone production efficiency and NO_x depletion in an urban plume: Interpretation of field observations and implications for evaluating O_3-NO_x-VOC sensitivity, J. Geophys. Res.-Atmos., 108, 23, https://doi.org/10.1029/2002jd003144, 2003.

Zhang, C. X., Liu, C., Hu, Q. H., Cai, Z. N., Su, W. J., Xia, C. Z., Zhu, Y. Z., Wang, S. W., and Liu, J. G.: Satellite UV-Vis spectroscopy: implications for air quality trends and their driving forces in China during 2005-2017, Light-Sci Appl, 8, 12, https://doi.org/10.1038/s41377-019-0210-6, 2019.

https://doi.org/10.5194/acp-2020-1298
Preprint. Discussion started: 25 February 2021

Zhang, Q., Streets, D. G., He, K., Wang, Y., Richter, A., Burrows, J. P., Uno, I., Jang, C. J., Chen, D., Yao, Z., and Lei, Y.: NO_x emission trends for China, 1995-2004: The view from the ground and the view from space, J. Geophys. Res.-Atmos., 112, 18, https://doi.org/10.1029/2007jd008684, 2007.

Zhu, L., Jacob, D. J., Keutsch, F. N., Mickley, L. J., Scheffe, R., Strum, M., Abad, G. G., Chance, K., Yang, K., Rappengluck, B., Millet, D. B., Baasandorj, M., Jaegle, L., and Shah, V.: Formaldehyde (HCHO) As a Hazardous Air Pollutant: Mapping Surface Air Concentrations from Satellite and Inferring Cancer Risks in the United States, Environ Sci Technol, 51, 5650-5657, https://doi.org/10.1021/acs.est.7b01356, 2017a.

Zhu, L., Mickley, L. J., Jacob, D. J., Marais, E. A., Sheng, J. X., Hu, L., Abad, G. G., and Chance, K.: Long-term (2005-2014) trends in formaldehyde (HCHO) columns across North America as seen by the OMI satellite instrument: Evidence of changing emissions of volatile organic compounds, Geophys Res Lett, 44, 7079-7086, https://doi.org/10.1002/2017gl073859, 2017b.